Journal of Materials Chemistry C

RSC Publishing

PAPER

View Article Online
View Journal | View Issue

Cite this: J. Mater. Chem. C, 2013, 1, 5133

Selective-swelling-induced porous block copolymers and their robust TiO_2 replicas *via* atomic layer deposition for antireflective applications

Jie Yang,[a] Ling Tong,[a] Yang Yang,[a] Xiaoqiang Chen,[a] Jun Huang,[a] Rizhi Chen[ab] and Yong Wang*[a]

We prepared antireflective nanoporous membranes by an extremely simple method which only involves the immersion of the optical substrates coated with amphiphilic block copolymers in hot ethanol for hours and a subsequent air drying process. Nanometer-sized pores were formed throughout the copolymer films through the swelling-induced pore generation mechanism. The pore structure and size, and consequently the antireflective properties of the porous copolymer membranes, could be modulated by changing the concentrations of the copolymer solutions and also the swelling temperature and time. A transmittance higher than 99% of the copolymer-coated glass substrate could be obtained at optimized conditions. Furthermore, to obtain robust and easily cleanable antireflective layers, we deposited TiO_2 on the porous copolymer membranes by atomic layer deposition followed by calcination in air to burn off the polymer components, producing highly porous TiO_2 membranes composed of interconnected nanotubes with thin tube walls. The replicated TiO_2 membranes also displayed a good antireflective function because of their high porosity. Thanks to the conformal deposition of TiO_2 on the copolymer membranes, the TiO_2 replicas maintained structural integrity and mechanical robustness after high temperature calcination, and were tightly adhered to the glass substrate. Moreover, the calcined TiO_2 was transformed to anatase and exhibited a photocatalytic effect. We demonstrated that contaminated TiO_2 layers could recover their original high transmittance, either by directly rinsing with water or organic solvents, or by UV exposure to degrade organic contaminants.

Received 29th April 2013
Accepted 17th June 2013

DOI: 10.1039/c3tc30802b

www.rsc.org/MaterialsC

1 Introduction

Antireflective (AR) layers have been widely applied on the optical surfaces of lenses, photovoltaic cells, detectors, displays, *etc.* to suppress the reflection of light at the interfaces between the substrate and air, or other media the substrate is exposed to.[1–5] According to the well-known Fresner formula,[6] to obtain complete elimination of the reflection, the AR layer needs to meet two criteria: (1) a refractive index (n_1) fulfilling the equation $n_1 = (n_0 n_2)^{1/2}$, where n_0 and n_2 are the refractive indices of the medium in which the substrate is exposed, *e.g.*, air and the substrate, respectively, and (2) a thickness equal to one quarter of the light wavelength in the medium. For a glass substrate with $n_2 = 1.52$, the ideal n_1 of an AR layer which exhibits zero reflectance can be deduced to be 1.23 if this optical component is going to be used in air with $n_0 = 1$. However, a homogeneous layer of any existing material can only reach a lowest n_0 of $\sim$1.35. The typical solution is to create air gaps inside the AR layer approaching $n_1 = 1.23$, as air has the lowest refractive index. n_1 of the AR layer with air gaps can be tuned from the refractive index value of air and that of the matrix material by changing the volume of the air gaps.

Air gaps mean porosity inside the material matrix. Therefore, AR layers are typically porous membranes with high porosity. To avoid light scattering inside the AR layer the pore size needs to be smaller than the wavelength of the incident light. Porous membranes of both polymeric and inorganic materials have been used as AR layers as they have their own advantages over other types. For example, polymeric AR layers are easy to be processed, whereas AR layers of metal oxides possess a strong chemical and thermal resistance. A number of strategies, including the demixing of polymer blends,[7] layer-by-layer assembly of different polymer thin films,[8] microphase separation of block copolymers (BCPs),[9–13] *etc.* have been developed to prepare porous polymeric AR layers. Among these methods, microphase separation of BCPs is distinctive as it produces well-defined periodic morphologies with a feature sizes in the range of 10–100 nm.[14] Selective removal of the dispersed phases leads to porous structures with corresponding sizes.[15,16] Moreover, the

[a]State Key Laboratory of Materials-Oriented Chemical Engineering, College of Chemistry and Chemical Engineering, Nanjing University of Technology, Nanjing, 210009 Jiangsu, China. E-mail: yongwang@njut.edu.cn

[b]Jiangsu Key Laboratory of Industrial Water-Conservation & Emission Reduction, Nanjing University of Technology, Nanjing, 210009 Jiangsu, China

porosity and consequently the light transmittance of the BCP-derived membranes can be easily tuned by using BCPs with different fractions of the minor blocks. Kim *et al.* pionnered the BCP-based AR layers.[12] They used diblock copolymers of polystyrene and poly(methyl methacrylate) (PS-*b*-PMMA) as the PMMA domains could be selectively removed by UV light exposure followed by rinsing with acetic acid and converting into spongy-like porous structures contained in the crosslinked PS matrix. The obtained PS layer showed an excellent AR performance with a nearly 100% transmittance at a specific wavelength.[12] Moreover, by constructing multiple PS layers with different pore sizes derived from PS-*b*-PMMA having various block lengths, they obtained broadband AR layers.[13] Alternatively, Han and coworkers used the nonsolvent-induced phase separation method to prepare porous layers of diblock copolymers of PS and poly(4-vinyl pyridine) (PS-*b*-P4VP) showing excellent AR function.[14] They were also able to construct a gradient porosity in the BCP film which exhibited a broadband AR property using blends of PS-*b*-PMMA and PMMA homopolymers.[15,16]

The polymeric AR layers suffer poor resistance to abrasion, chemicals, and heat although they have a good processability and controllability in pore structures.[17] In contrast, inorganic materials, mainly metal oxides including SiO_2 and TiO_2 are frequently used to build mechanically robust AR coatings. Such AR layers of metal oxides are usually prepared by methods including sol gel,[18,19] densely packing of nanoparticles,[20] magnetron sputtering,[21] hydrothermal treatment,[22] anodization,[23] *etc.* However, it is typically difficult to finely tune the pore structure of the inorganic AR layers. Therefore, it should be very interesting to have a preparative method to AR layers combining the advantages of both the polymeric and inorganic materials. In this work, we first demonstrated that nanoporous polymeric membranes produced by the selective swelling of amphiphilic BCPs of PS and poly(2-vinyl pyridine) (PS-*b*-P2VP) showed a tunable AR function. We then used the porous BCP membranes as templates and deposited TiO_2 on their pore walls by atomic layer deposition, which was distinguished from other methods for its conformal and uniform deposition on the surface of fine pores in a cyclic mode.[24,25] Following calcination in air that burned off the BCP template a highly porous TiO_2 membrane was yielded composed of interconnected nanotubes. The TiO_2 membranes showed a good AR property and they were mechanically robust and possessed a photocatalytic effect which allows cleaning by washing with liquids under ultrasonication, or self-cleaning with UV light.

2 Experimental section

Preparation of nanoporous PS-*b*-P2VP membranes

PS-*b*-P2VP [M_n (PS) = 50 000 g mol^{-1}; M_n (P2VP) = 16 500 g mol^{-1}] was purchased from Polymer Source and was used without further purification. The BCP was dissolved in chloroform at the desired concentrations. The obtained BCP solutions were filtrated three times through PTFE filters with a nominal pore size of 0.22 μm to remove any big aggregates. BCP solutions were spin-coated (5000 rpm for 40 s) onto cleaned silicon or K9 glass substrates (Nantong zhenhua optical-electric Co., Ltd). The BCP-coated substrates were then immersed in ethanol to carry out the swelling-induced pore generation process at a preset temperature for desired periods of time.

Fabrication of TiO_2 replicas from porous BCP templates by ALD

The ALD was performed in a commercial reactor (Savannah 100, Cambridge NanoTech) at a temperature of 80 °C. The reactor chamber with BCP templates inside was heated to the deposition temperature and pumped to reach a pressure <1 torr. $TiCl_4$ (>99.99%, Aladdin Reagents) and deionized water were used as the precursors. The chamber was kept pumping at the deposition temperature for at least 30 min before pulsing precursor vapors. Precursor vapors were pulsed into the chamber using nitrogen as the carrying gas at a flow rate of 20 sccm. Each precursor pulse was followed by a gas purge of pure nitrogen also at 20 sccm. We adopted the exposure mode to ensure an adequate diffusion time for precursors to penetrate into the fine pores in BCP templates, which means the precursor vapors were held for an exposure time (ET) in the reactor before they were purged away. A typical ALD cycle in this work can be described as "$TiCl_4$/ET/N_2/H_2O/ET/N_2 = 0.03 s/10 s/40 s/0.015 s/10 s/40 s". The templates were subjected to prescribed numbers of ALD cycles. To degrade the BCP templates, the deposited BCP membranes were heated to 450 °C in air at a rate of 3 °C min^{-1} and kept at this temperature for 3 h and then cooled down to room temperature naturally.

Characterization

Surface and cross-sectional morphologies of different samples were examined with a field emission scanning electron microscope (Hitachi S4800) operated at 2 or 5 kV. Prior to SEM observation, the samples were sputter-coated with a thin layer of gold/palladium alloy. The transmittance in the wavelength range of 400–2000 nm of the pristine and coated glass substrates was obtained from a UV-vis-NIR spectrophotometer (Lambda 950, Perkin Elmer). In the measurement of transmittance, both sides of the glass substrate were treated to have either a layer of porous BCP or TiO_2. The refractive index and thickness of the porous membranes of BCP and TiO_2 prepared at different conditions were measured with a spectroscopic ellipsometer (Complete EASE M-2000U, J. A. Woollam) with a 632.8 nm laser at a 70° incident angle. XRD patterns of the TiO_2-coated BCP membranes before and after calcination were recorded from a desktop diffractometer (Miniflex 600, Rigaku). A contact angle goniometer (Dropmeter A-100, Maist) was used to detect the water contact angles of both porous polymeric and TiO_2 films and the average value of the measurements at five different positions on the sample surface was reported. To investigate the mechanical stability of TiO_2 replica films, the 60-cycle TiO_2 replica film deposited on the glass substrate was immersed in water and ultrasonicated for 10 min at a power of 100 W and an ultrasound frequency of 40 kHz. We used two different ways to clean the contaminated TiO_2 AR layers: rinsing with liquids and photocatalytic degradation. Rhodamine B and

oleic acid were chosen as the representative water-soluble and water-insoluble contaminants, respectively. To purposely contaminate the TiO_2 AR layer, the glass substrate with a porous TiO_2 AR layer prepared at 60 ALD cycle number was immersed in either the aqueous solution of Rhodamine B (100 mg L^{-1}) or the acetone solution of oleic acid (1 wt%) for 3–5 min followed by air drying to remove the solvent and leave Rhodamine B or oleic acid adsorbed on the TiO_2 layers. In the adsorption of Rhodamine B, the immersion and drying process were repeated twice to ensure an adequate adsorption of Rhodamine B. The Rhodamine B- and oleic oil-adsorbed AR layers were then cleaned by rinsing in deionized water and acetone for several minutes. The transmittance of the contaminated porous TiO_2-coated substrates before and after cleaning with liquids was measured to investigate the transmittance recovery through the liquid cleaning method. In addition, the Rhodamine B-adsorbed porous TiO_2 AR layer supported on the glass substrate was also irradiated with ultraviolet light (365 nm, 3 mW cm^{-2}) for different times and the change of its transmittance with the irradiation time was recorded to evaluate the effect of cleaning by photocatalysis.

3 Results and discussion

We first prepared nanoporous polymeric membranes with tunable thicknesses and pore sizes by selective swelling of the amphiphilic BCPs spincoated on glass substrates. BCP solutions with different concentrations ranging from 0.6% to 1.2% were spincoated on the glasses, generating nonporous BCP films with varying thicknesses on the glasses. The BCP-coated glass slides were then immersed in ethanol at 65 °C for 15 h, followed by air drying at room temperature after withdrawal of the slides from the ethanol bath. As shown in Fig. 1, all the samples prepared from different BCP concentrations exhibited a highly porous morphology. The membranes were mainly composed of two types of pores: circular pores with a diameter less than 50 nm (highlighted in the circle) and irregular pores with sizes scattering in the range of ~50 to 300 nm (highlighted in the square). Moreover, we can observe some circular pores through large irregular pores, implying the interconnected nature of the pores distributed in different thicknesses of the membrane. The irregular pores gradually evolved to a channel-like shape with the channel width close to the diameter of the circular pores when the concentration of the BCP solutions increased from 0.6% to 1.2% (Fig. 1d). In other words, higher concentrations of BCP solutions led to more homogeneous pores with a narrow pore size distribution, which can be understood by the formation mechanism of these pores.

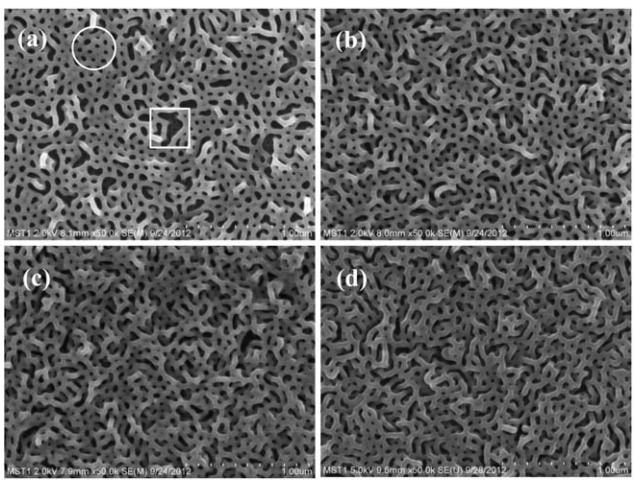

Fig. 1 SEM images of the surface morphology of porous membranes obtained from BCP solutions with different concentrations: (a) 0.6%; (b) 0.8%; (c) 1.0%; (d) 1.2%. The porous membranes were prepared by swelling the spincoated BCP films in ethanol at 65 °C for 15 h, followed by air drying at room temperature.

These porous structures were formed through a swelling-induced pore generation mechanism.[26,27] PS-*b*-P2VP was molecularly dissolved in chloroform because chloroform is a neutral solvent for both PS and P2VP blocks. Microphase separation of the copolymer occurred with the fast evaporation of chloroform during the spincoating process, forming P2VP cylinders randomly distributed throughout the PS matrix. When the BCP film was immersed in ethanol, ethanol molecules were selectively enriched in the P2VP cylinders and the P2VP chains were swollen because ethanol possessed a strong affinity to P2VP generating osmotic pressure inside the P2VP cylinders surrounded by the PS matrix. The accumulated osmotic pressure forced the PS matrix to deform as the PS chains had an enhanced mobility as the swelling was carried out at 65 °C. In the following air drying at room temperature, the deformed PS matrix could not recover its original position because the PS chains were frozen at room temperature, that is, the expanded spaces occupied by the swollen P2VP chains were preserved. However, the swollen P2VP chains collapsed due to the evaporation of ethanol, producing pores in the positions of the original P2VP cylinders with the pore walls covered by the collapsed P2VP chains. The P2VP cylinders oriented perpendicularly and in parallel to the film surface and were converted to circular and channel-like pores, respectively. In the swelling process, neighbouring P2VP cylinders contacted and connected with each other, resulting in the three dimensionally interconnected nature of the pores after drying. For the BCP films prepared from solutions with lower concentrations, fewer P2VP cylinders were formed in the spincoating process and they had less constraint to expand from their neighbours. Consequently, they had more space to expand their sizes and were converted to pores with larger sizes and irregular shapes. In contrast, for the films prepared from higher concentrations, the densely distributed P2VP cylinders limited their expansion by each other, leading to a more homogeneous pore morphology.

Fig. 2 displays the transmittance spectra of the glass substrates coated with porous BCP membranes prepared from different BCP concentrations. The glass substrate exhibited a transmittance that slightly varied in the range of 91–92% when the wavelength of the incident light increased from 400 nm to 1600 nm. All the glass substrates coated by porous BCP membranes demonstrated an enhanced transmittance. Nanoporous membranes prepared from higher BCP concentrations yielded greater transmittance. For instance, the porous membrane obtained from the concentration of 0.6% showed a

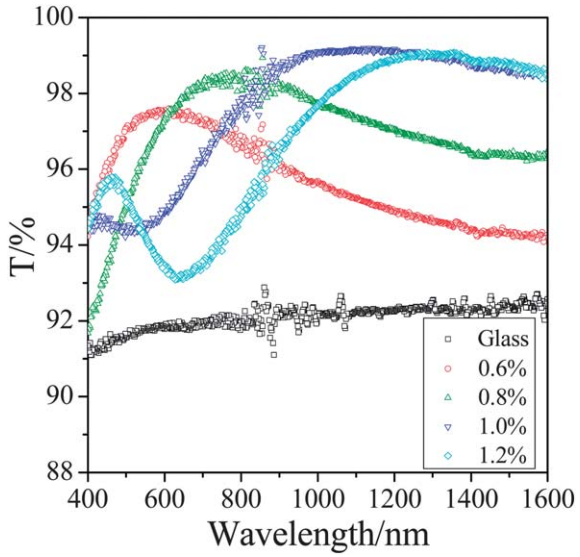

Fig. 2 Transmittance spectra of the porous BCP membranes prepared with different BCP concentrations.

maximum transmittance (T_{max}) of 97.6%, whereas the T_{max} of the membrane from 1.0% BCP solution was 99.2%. The better transmittance of the membranes prepared from higher BCP concentrations is attributed to their more uniform pores as irregular big pores were present in the BCP membranes prepared from the concentration of 0.6% scattered incident light. We measured the thickness and refractive index of the porous BCP membranes prepared from BCP concentrations using ellipsometry, which is summarized in Table 1 together with their T_{max}. The thickness of the spincoated BCP films increased with the BCP concentration, and the wavelengths at which the maximum transmittance appeared correspondingly shifted to higher values. Therefore, we could conveniently realize the enhanced transmission at a specific wavelength by altering the concentration of the starting BCP solution. Moreover, as clearly revealed by Fig. 1 the porosity of the porous membranes decreased with the BCP concentration, leading to an increasing refractive index with the rise of the BCP concentration because less air was included in the BCP membranes.

We then investigated the influence of swelling temperature and time on the pore structure of the membrane and consequently their antireflection performances. When the swelling temperature was low, *e.g.* 55 °C, the mobility of the PS chains was slightly enhanced and most P2VP cylinders could not adequately expand because of the tight constraints of the PS matrix. Therefore, only a few small pores were formed after drying, as shown in Fig. 3a–c. Increasing the swelling time from 6 h to 15 h or 24 h slightly increased the number and size of pores. As shown in Fig. 3d, the porous membranes obtained by swelling at 55 °C for different times all displayed enhanced transmittance and the degree of the transmittance enhancement increased with the swelling time. For example, T_{max} increased from 93.8% at a swelling time of 6 h to 97.2% and 98.4% at a swelling time of 15 h and 24 h, respectively. Such a rise of T_{max} was directly related to the increasing porosity of the membranes with extending swelling times. When the swelling temperature increased to 65 °C, pores formed at a much faster rate because of the significantly enhanced mobility of PS chains and a large number of circular pores and irregular pores could be observed on the surface of the membrane subjected to swelling for 6 h (Fig. 3e). As a consequence of this a large number of pores appeared in the BCP membrane, the membrane showed a good AR performance with a T_{max} of 98.8%. Extending the swelling time to 15 h slightly improved the T_{max} to 99.2% because of the increased porosity as clearly revealed by the SEM images (Fig. 3f and g). However, further prolonging the swelling time to 24 h did not yield an even higher T_{max}. On the contrary, the T_{max} of the 24 h swelling-treated membrane dropped to 98.9%. This is attributed to the presence of larger pores as a result of the strong swelling degree which scattered some incident light. At a swelling temperature of 75 °C, the membrane already showed a highly porous structure after a swelling time of 6 h. Extending the swelling temperature to 15 h and 24 h enlarged the pore size and more big pores appeared. As these big pores scattered the incident light, the membranes showed a slightly decreasing transmittance with increased swelling time (Fig. 3l). Therefore, we conclude that the AR performances could be enhanced by increasing the porosity of the membrane *via* elevating the swelling temperature and/or extending the swelling time. However, strong degrees of swelling as a result of higher swelling temperatures or longer swelling times should be avoided as they may produce large pores which scatter a certain portion of incident light and weaken the AR performance.

To obtain robust AR coatings with an additional self-cleaning function we transformed the porous BCP membranes to porous TiO_2 membranes by atomic layer deposition of TiO_2 on the BCP membranes which were subsequently burned off. TiO_2 was chosen as the target material because of its superior chemical and thermal resistance and photocatalytic function to degrade organic compounds.[28] Fig. 4 exhibits the surface morphology of the porous TiO_2 membranes prepared at different ALD cycles. When the ALD cycle number was low, *e.g.* 40, the obtained TiO_2 showed a collapsed structure composed of mainly broken tubes (Fig. 4a). However, when the cycle number increased to higher than 50, the interconnected network structure of the BCP template membranes was preserved, whereas the pore size progressively decreased with increasing ALD cycle numbers (Fig. 4b–d). Examination of the cross-sections of the obtained TiO_2 networks revealed that these

Table 1 The refractive index (n), thickness, and T_{max} and the corresponding wavelength of porous BCP membranes prepared with different BCP concentrations

Concentration	n	Thickness/nm	T_{max}	Wavelength with T_{max}/nm
0.6%	1.17	142	97.6%	612
0.8%	1.19	193	98.4%	814
1.0%	1.21	201	99.2%	1120
1.2%	1.21	326	99.0%	1290

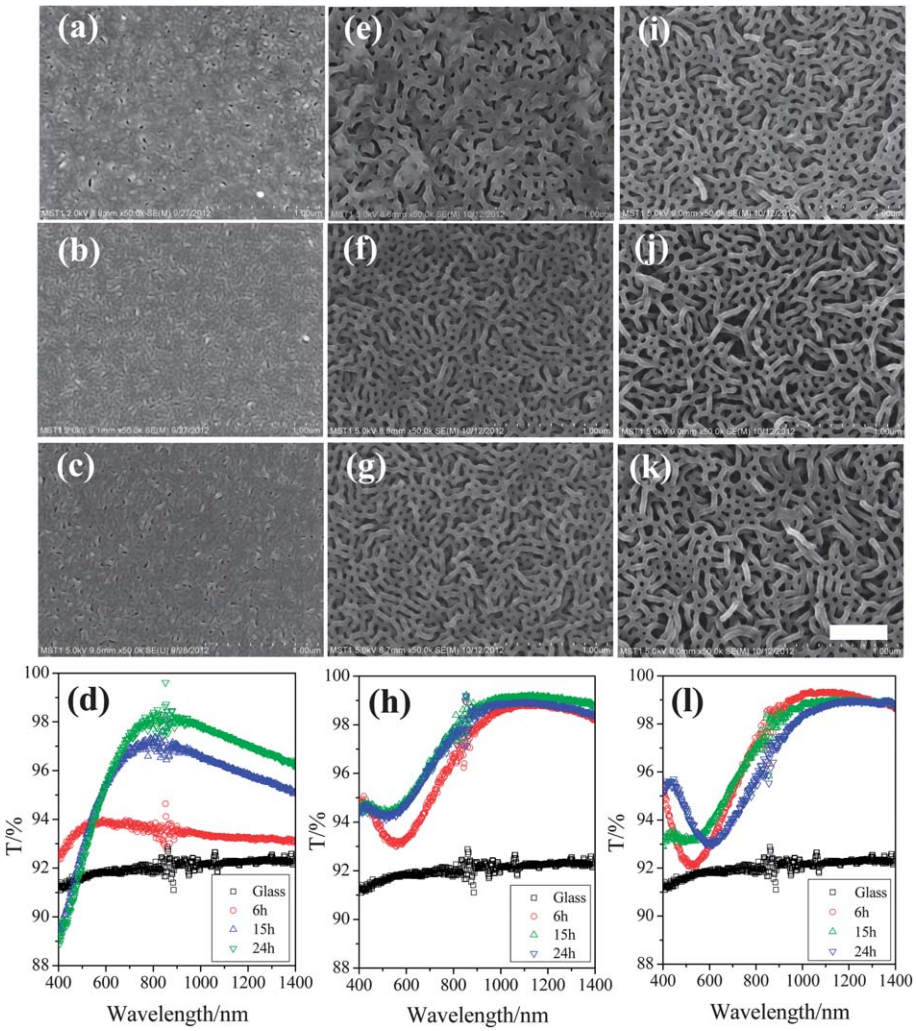

Fig. 3 SEM images of the surface morphology and transmittance spectra of porous BCP membranes prepared at different swelling temperatures and times. The swelling temperatures of (a–d), (e–h), and (i–l) were 55 °C, 65 °C, and 75 °C, respectively. The swelling times of (a, e, i), (b, f, j), and (c, g, k) were 6 h, 15 h, and 24 h, respectively. All these BCP membranes were obtained from BCP solutions with a concentration of 1%. All of the SEM images have the same magnification and an additional enlarged scale bar corresponding to 500 nm is shown in (k).

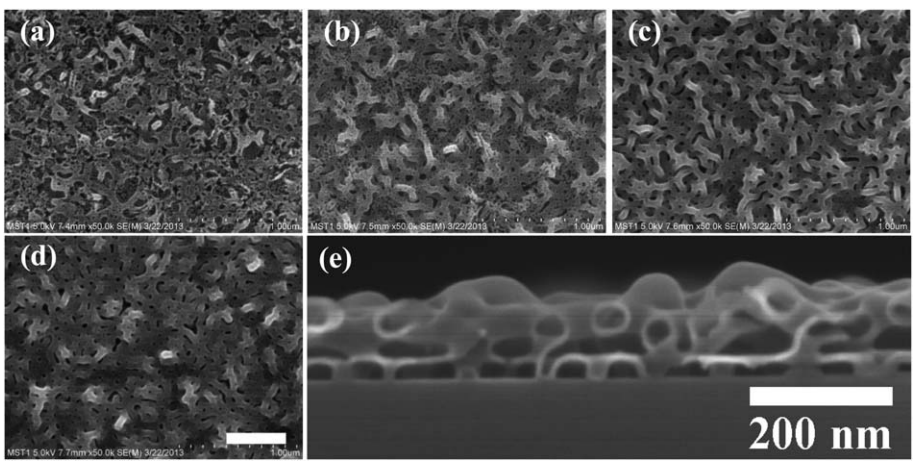

Fig. 4 SEM images of the surface (a–d) and cross-section (e) of porous TiO_2 networks prepared by ALD on BCP templates with different ALD cycle numbers: (a) 40 cycles, (b) 50 cycles, (c and e) 60 cycles, (d) 70 cycles. The BCP templates were prepared by spincoating the 0.6% BCP solution on glass substrates followed by swelling at 65 °C for 15 h. Pannels (a–d) have the same magnification and an additional enlarged scale bar corresponding to 500 nm is shown in (d).

network structures were composed of interconnected tubes with hollow interiors (Fig. 4e). In the ALD process, TiO_2 was uniformly grown along the pore walls of the porous BCP membranes as vaporized precursors ($TiCl_4$ and water) easily diffused into the small pores and adsorbed and reacted on the pore walls. Conformal thin layers of TiO_2 partially infiltrating in the P2VP layer of the BCP templates were produced because the sequential infiltration of the precursors also occurred in the early stage of TiO_2 deposition.[29,30] Subsequent calcination in air decomposed the BCP template, leaving behind the TiO_2 replica containing void spaces originally occupied by the polymer skeleton. The thickness of the deposited TiO_2 layer could be simply increased by repeating the ALD cycles. At low cycle numbers, for example, 40 and 50 cycles, the thickness of the produced TiO_2 was too thin to withstand the high temperature calcination, yielding a collapsed TiO_2 structure or porous defects in the tube wall. We then checked the AR performances of the TiO_2 membranes prepared at different ALD cycles. As shown in Fig. 5, the 40-cycles-TiO_2 membrane showed a slightly enhanced AR property because of its collapsed structure. Increasing the cycle number from 40 to 50 and 60 led to a continuous rise in T_{max}. whereas an even higher cycle number of 70 gave a decreased T_{max}. Larger cycle numbers produced thicker TiO_2 layers and reduced the size of gaps between the tubes comprised of the TiO_2 membrane, which contributed to less porosity of the TiO_2 membrane. However, thicker tube walls endowed the TiO_2 membrane with a stronger mechanical stability and less shrinkage occurred in the calcination. The smaller amount of dimensional shrinkage of the membranes with a higher number of ALD cycles was evidenced by the thickness of the TiO_2 membranes in comparison with their corresponding BCP templates. The porous BCP template had a thickness of ~150 nm, whereas the TiO_2 membranes prepared at 50, 60, and 70 cycles on the same BCP template exhibited thicknesses of 82, 92, and 98 nm, respectively. Note that the thickness of the ALD-deposited BCP membranes with a cycle number of 40 or 70 did not noticeably change as the ALD of TiO_2 proceeded at a very low growth rate (several Ångstrom per cycle)[24] and several tens of ALD cycles just increased the membrane thickness by several nanometers which could be neglected compared to a thickness of 142 nm of the BCP membrane. Consequently, the TiO_2 membranes with a thicker tube wall tended to have higher porosity than those having a thinner tube wall. The competing effect of the thicker tube wall and less shrinkage resulted in the increase in T_{max} when the cycle number increased from 40 to 60 and a following decrease with the further increase of cycle number from 60 to 70. The AR effect of the TiO_2 membrane deposited on the glass substrate could be directly demonstrated by the photographs of a bare glass substrate and a deposited one. As shown in Fig. 5b, the TiO_2-deposited glass showed a higher transparency than the bare one.

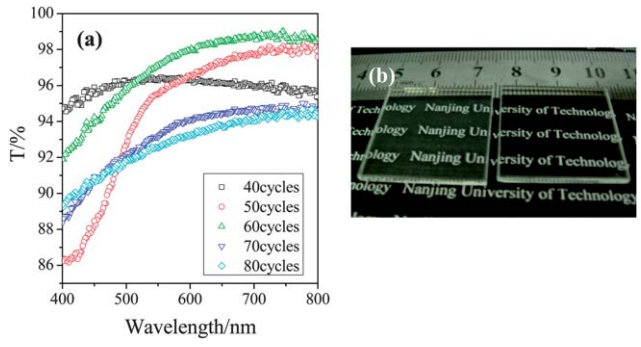

Fig. 5 (a) Transmittance spectra of porous TiO_2 membranes prepared from a BCP template with different numbers of ALD cycles. (b) The photograph of a bare glass substrate (left) and a glass substrate with a TiO_2 membrane coating layer prepared at 60 ALD cycles (right).

We compared the AR performances of the TiO_2 replicating structures and the porous BCP membranes. The BCP templates had a relatively low transmission, like the one produced from a 0.6% BCP solution and a swelling temperature of 65 °C and time of 15 h, the TiO_2 replica may obtain an improved transmittance. For example, the 60-cycle-TiO_2 replica exhibited approximately 1% higher transmittance in the wavelength range of 500 nm to 800 nm than its counterpart BCP template. This further increase in transmittance should be attributed to the hierarchical pore structure of the TiO_2 membranes. In addition to pores defined by the gaps among the tubes, the hollow interiors of the tubes also significantly increased the porosity of the TiO_2 membranes. The transmittance enhancement of the porous TiO_2 membranes given by their high porosity, however, was compromised by the very high refractive index of TiO_2 ($n = 2.52$ and 2.76 for anatase and rutile, respectively).[31] We also prepared TiO_2 membranes using BCP membranes which already had high transmittance as templates, but the transmittance of the obtained TiO_2 replica was not further improved to be better than that of the porous BCP templates because the increased porosity could not offset the increased refractive index of TiO_2 compared to the polymer. We challenged the TiO_2-deposited glass substrate with a harsh ultrasonication oscillation at a power of 100 W for 10 min and found its transmittance spectrum remained almost unchanged before and after ultrasonication (Fig. 6). The nondeteriorated AR performance implied that the TiO_2 membranes were mechanically robust and tightly adhered to the glass substrate, although their comprising tubes had very thin tube walls with a thickness of a few nanometers.[32] Such a strong mechanical stability was believed to originate from the interconnected, network-like structure of the TiO_2 membranes. The strong mechanical robustness of the TiO_2 membranes together with the chemical resistance to acids, bases, and organic solvents of TiO_2 materials allowed the contaminated TiO_2-coated substrates to be cleaned by directly rinsing with liquids and even with the assistance of ultrasonification, which would be highly desirable in practical applications. We purposely contaminated the porous TiO_2 AR layers prepared at 60 ALD cycles with water-soluble Rhodamine B and water-insoluble oleic acid. As shown in Fig. 7a, the TiO_2-deposited glass slides contaminated by Rhodamine B showed significantly reduced transmittance at wavelengths around 560 nm, because of the high levels of adsorption of Rhodamine B. Fortunately, rinsing in water for

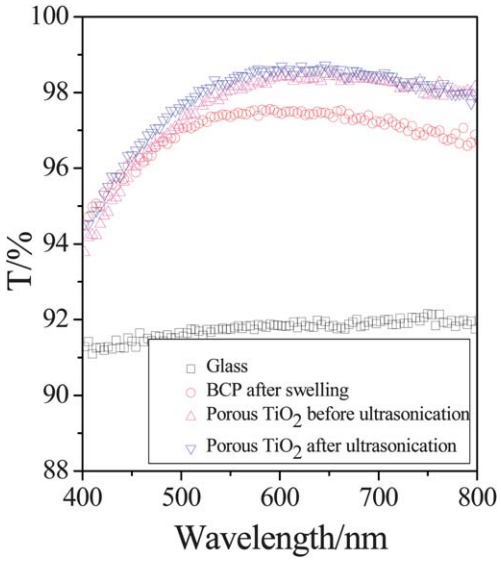

Fig. 6 The transmittance spectra of the porous BCP membrane prepared by spincoating the 0.6% BCP solution on the glass substrate followed by swelling at 65 °C for 15 h and the TiO_2 membrane prepared by ALD deposition of TiO_2 on the above-mentioned BCP membrane with 60 cycles before and after the ultrasonication treatment.

several minutes recovered most of the transmittance as Rhodamine B molecules had been desorbed from the porous TiO_2 layer and dissolved in water. The strong hydrophilicity of the porous TiO_2 films[33], which exhibited a water contact angle (WCA) of ~30°, facilitates the penetration of water into the fine and tortuous pore structure of the films, leading to an effective rinsing away of the adsorbed contaminants and correspondingly a quick recovery of the transmittance. In contrast, most polymer films are much more hydrophobic than TiO_2, for example, the porous BCP films have a WCA of ~70°, therefore water rinsing to recover their transmittance will not be as effective as the case of the porous TiO_2 films. However, there are also oleophilic contaminants and rinsing in water may not recover the AR performance. As shown in Fig. 7b, the oleic acid-contaminated glass slide with the porous TiO_2 AR layer totally lost its AR function and its transmittance was lower than 89%, which was even poorer than the bare glass slide because of the oleic acid liquid film adsorbed on the TiO_2 layer. Rinsing in water just slightly improved the transmittance by approximately 1% because of the poor solubility of oleic acid in water. However, rinsing in acetone resulted in a nearly complete recovery of the transmittance in the entire range of wavelength studied.

Alternatively, in the case of cleaning with liquids this is not convenient for organic contaminants on the TiO_2 AR layer that can also be removed by a "dry" process, as TiO_2 in the anatase form exhibited a photocatalytic effect in decomposing organic compounds. X-ray diffraction analysis revealed that the TiO_2 membrane was transformed to the anatase form during the high temperature calcination procedure from the amorphous state before calcination (Fig. 8a). As shown in Fig. 8b, UV exposure gradually decomposed the Rhodamine B molecules adsorbed on the porous TiO_2 AR layer and the transmittance of the glass slide was progressively recovered. Therefore, the robustness of the porous TiO_2 structures allows recovery of the transmittance of the AR layers by directly rinsing with water or organic solvents, and the photocatalytic effect of anatase TiO_2 makes it possible to regenerate the transmittance by photodegrading the organic contaminants on the AR layers. In contrast we found that the contaminated porous BCP film only exhibited a very slight increase in transmittance after exposure to UV light for 2 h (from 80% to 83%) because the BCP film did not have a photocatalytic effect. Such a slight increase in transmittance might be due to the self-decomposition of Rhodamine B under a long-time exposure of UV light. Moreover, exposure of polymer films to UV light for extended time might cause the decomposition of the polymer itself, which will lead to the collapse of the porous structure and correspondingly the AR function. Therefore, rinsing with organic solvents and UV exposure should not be used to clean AR layers composed of polymers as their porous structures are prone to be destroyed by organic solvents or UV light which leads to the loss of their AR function. Additionally, we may further enhance the photocatalytic effect to have a faster cleaning of the contaminated TiO_2 films by optimizing the porosities of the TiO_2 films, as there is a correlation between the porosity and photocatalytic effectiveness of the porous TiO_2 films.[34,35]

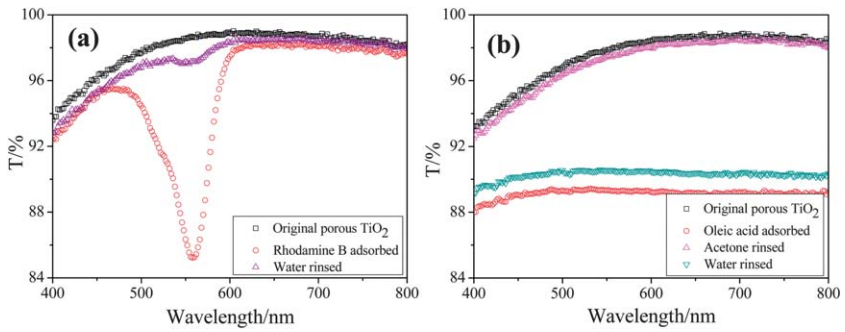

Fig. 7 Transmittance spectra of the porous TiO_2 membrane prepared at an ALD cycle number of 60 contaminated by the adsorption of Rhodamine B and cleaned by rinsing with water (a), and transmittance spectra of this porous TiO_2 membrane contaminated by the adsorption of oleic acid and cleaned by rinsing with acetone (b).

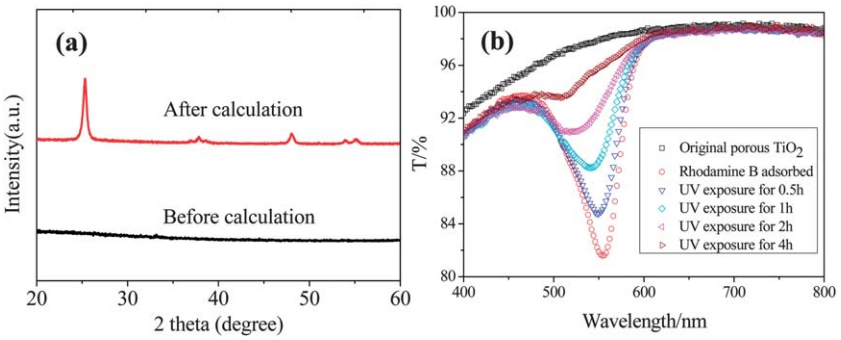

Fig. 8 (a) XRD patterns of the porous BCP membrane subjected to 80 TiO_2 ALD cycles before and after calcination in air at 450 °C. (b) Transmittance spectra of the porous TiO_2 membrane prepared at an ALD cycle number of 60 contaminated by the adsorption of Rhodamine B and cleaned by UV exposure for different times.

4 Conclusions

We demonstrated that nanoporous polymeric membranes can be easily prepared by selective swelling of amphiphilic block copolymers and which exhibited a good antireflective function because of their interconnected pore structure. This swelling-based method to antireflective coating is distinctive for its simplicity and nondestructive nature. The thickness, pore morphology, and porosity of the porous membranes could be tuned by changing the concentration of the starting BCP solution and the swelling temperature and time, allowing easy control of the refractive index and the wavelength at which the highest transmittance occurred. Furthermore, the thus obtained porous membranes were employed as templates from which TiO_2 replicas were obtained by atomic layer deposition. The TiO_2 replicas also exhibited enhanced light transmittance because of their high porosity. The porous TiO_2 replica tightly adhered to the substrate surface and showed a strong mechanical robustness which tolerated rigorous ultrasonication oscillation. Moreover, the porous TiO_2 replicas exhibited a photocatalytic effect. We demonstrated that the AR performance of the contaminated TiO_2 replicas could be recovered either by direct cleaning with water, or organic solvents, or by self-cleaning with UV light exposure.

Acknowledgements

Financial support from the National Basic Research Program of China (2011CB612302), the Natural Science Foundation of China (21176120 and 21004033), the Doctoral Program Foundation of Institutions of Higher Education of China (20123221110003), the Jiangsu Natural Science Funds for Distinguished Young Scholars (BK2012039), the Fok Ying Dong Education Foundation (131046), and the Natural Science Foundation of the Jiangsu Higher Education Institutions is gratefully acknowledged.

References

1 J. Hiller, J. D. Mendelsohn and M. F. Rubner, *Nat. Mater.*, 2002, **1**, 59.
2 S. Diedenhofen, G. Vecchi, R. E. Algra, A. Hartsuiker, O. L. Muskens, G. Immink, E. P. A. M. Bakkers, W. L. Vos and J. G. Rivas, *Adv. Mater.*, 2009, **21**, 973.
3 W.-L. Min, B. Jiang and P. Jiang, *Adv. Mater.*, 2008, **20**, 3914.
4 J. Zhu, Z. F. Yu, G. F. Burkhard, C. M. Hsu, S. T. Connor, Y. Q. Xu, Q. Wang, M. McGehee, S. H. Fan and Y. Cui, *Nano Lett.*, 2009, **9**, 279.
5 S. J. Cho, T. An, J. Y. Kim, J. Sung and G. Lim, *Chem. Commun.*, 2011, **47**, 6108.
6 H. A. Macleod, *Thin Optical Filters*, Adam Hilger Ltd., Bristol, UK, 2nd edn, 1986.
7 S. Walheim, E. Schäffer, J. Mlynek and U. Steiner, *Science*, 1999, **283**, 520.
8 L. B. Zhang, Y. Li, J. Q. Sun and J. C. Shen, *Langmuir*, 2008, **24**, 10851.
9 W. Joo, M. S. Park and J. K. Kim, *Langmuir*, 2006, **22**, 7960.
10 W. Joo, H. J. Kim and J. K. Kim, *Langmuir*, 2010, **26**, 5110.
11 X. Li and Y. C. Han, *J. Mater. Chem.*, 2011, **21**, 18024.
12 X. Li, L. Xue and Y. C. Han, *J. Mater. Chem.*, 2011, **21**, 5817.
13 X. Li, J. Gao, L. Xue and Y. C. Han, *Adv. Funct. Mater.*, 2010, **20**, 259.
14 F. S. Bates and G. H. Fredrickson, *Annu. Rev. Phys. Chem.*, 1990, **41**, 525.
15 M. A. Hillmyer, *Adv. Polym. Sci.*, **190**, 137.
16 D. A. Olson, L. Chen and M. A. Hillmyer, *Chem. Mater.*, 2008, **20**, 869.
17 X. Li, X. Yu and Y. C. Han, *J. Mater. Chem. C*, 2013, **1**, 2266.
18 J. Shen, T. Yang, Q. Zhang, J. Wang and Q. Zhang, *J. Sol-Gel Sci. Technol.*, 2003, **26**, 1029.
19 W. Joo, Y. Kim, S. Jang and J. K. Kim, *Thin Solid Films*, 2011, **519**, 3804.
20 Y. Du, L. E. Luna, W. S. Tan, M. F. Rubner and R. E. Cohen, *ACS Nano*, 2010, **4**, 4308.
21 W. Du, Y. P. Ye, H. X. Li, F. Zhao, L. Ji, W. L. Quan, J. M. Chen and H. D. Zhou, *Vacuum*, 2012, **86**, 1387.
22 Y. S. Tian, C. G. Hu, Y. F. Xiong, B. Y. Wan, C. H. Xia, X. S. He and H. Liu, *J. Phys. Chem. C*, 2010, **114**, 10265.
23 C.-T. Wu, C.-H. Lin, C. Cheng, C.-S. Wu, H.-C. Ting, F.-C. Chang and F.-H. Ko, *Chem. Mater.*, 2010, **22**, 6583.
24 S. M. George, *Chem. Rev.*, 2010, **110**, 111.
25 M. Knez, K. Niesch and L. Niinisto, *Adv. Mater.*, 2007, **19**, 3425.

26 Y. Wang, C. C. He, W. H. Xing, F. B. Li, L. Tong, Z. Q. Chen, X. Z. Liao and M. Steinhart, *Adv. Mater.*, 2010, **22**, 2068.
27 Y. Wang and F. B. Li, *Adv. Mater.*, 2011, **23**, 2134.
28 X. T. Zhang, O. Sato, M. Taguchi, Y. Einaga, T. Murakami and A. Fujishima, *Chem. Mater.*, 2005, **17**, 696.
29 Q. Peng, Y.-C. Tseng, S. B. Darling and J. W. Elam, *Adv. Mater.*, 2010, **22**, 5129.
30 Q. Peng, Y.-C. Tseng, S. B. Darling and J. W. Elam, *ACS Nano*, 2011, **5**, 4600.
31 X. T. Zhang, O. Sato, M. Taguchi, Y. Einaga, T. Murakami and A. Fujishima, *Chem. Mater.*, 2005, **17**, 696.
32 F. B. Li, X. P. Yao, Z. G. Wang, W. H. Xing, W. Q. Jin, J. Huang and Y. Wang, *Nano Lett.*, 2012, **12**, 5033.
33 A. Fujishima and K. Honda, *Nature*, 1972, **238**, 37.
34 L. Pinho and M. J. Mosquera, *J. Phys. Chem. C*, 2011, **115**, 22851.
35 L. Pinho and M. J. Mosquera, *Appl. Catal. B: Environmental*, 2013, **134–135**, 25.